

Observation of the Decay $B^0 \rightarrow \rho^+ \rho^-$ and Measurement of the Branching Fraction and Polarization

B. Aubert,¹ R. Barate,¹ D. Boutigny,¹ F. Couderc,¹ J.-M. Gaillard,¹ A. Hicheur,¹ Y. Karyotakis,¹ J. P. Lees,¹
V. Tisserand,¹ A. Zghiche,¹ A. Palano,² A. Pompili,² J. C. Chen,³ N. D. Qi,³ G. Rong,³ P. Wang,³ Y. S. Zhu,³
G. Eigen,⁴ I. Ofte,⁴ B. Stugu,⁴ G. S. Abrams,⁵ A. W. Borgland,⁵ A. B. Breon,⁵ D. N. Brown,⁵ J. Button-Shafer,⁵
R. N. Cahn,⁵ E. Charles,⁵ C. T. Day,⁵ M. S. Gill,⁵ A. V. Gritsan,⁵ Y. Groysman,⁵ R. G. Jacobsen,⁵ R. W. Kadel,⁵
J. Kadyk,⁵ L. T. Kerth,⁵ Yu. G. Kolomensky,⁵ G. Kukartsev,⁵ C. LeClerc,⁵ M. E. Levi,⁵ G. Lynch,⁵ L. M. Mir,⁵
P. J. Oddone,⁵ T. J. Orimoto,⁵ M. Pripstein,⁵ N. A. Roe,⁵ M. T. Ronan,⁵ V. G. Shelkov,⁵ A. V. Telnov,⁵
W. A. Wenzel,⁵ K. Ford,⁶ T. J. Harrison,⁶ C. M. Hawkes,⁶ S. E. Morgan,⁶ A. T. Watson,⁶ N. K. Watson,⁶
M. Fritsch,⁷ K. Goetzen,⁷ T. Held,⁷ H. Koch,⁷ B. Lewandowski,⁷ M. Pelizaeus,⁷ K. Peters,⁷ H. Schmuecker,⁷
M. Steinke,⁷ J. T. Boyd,⁸ N. Chevalier,⁸ W. N. Cottingham,⁸ M. P. Kelly,⁸ T. E. Latham,⁸ C. Mackay,⁸
F. F. Wilson,⁸ K. Abe,⁹ T. Cuhadar-Donszelmann,⁹ C. Hearty,⁹ T. S. Mattison,⁹ J. A. McKenna,⁹ D. Thiessen,⁹
P. Kyberd,¹⁰ A. K. McKemey,¹⁰ L. Teodorescu,¹⁰ V. E. Blinov,¹¹ A. D. Bukin,¹¹ V. B. Golubev,¹¹
V. N. Ivanchenko,¹¹ E. A. Kravchenko,¹¹ A. P. Onuchin,¹¹ S. I. Serednyakov,¹¹ Yu. I. Skovpen,¹¹ E. P. Solodov,¹¹
A. N. Yushkov,¹¹ D. Best,¹² M. Bruinsma,¹² M. Chao,¹² I. Eschrich,¹² D. Kirkby,¹² A. J. Lankford,¹²
M. Mandelkern,¹² R. K. Mommsen,¹² W. Roethel,¹² D. P. Stoker,¹² C. Buchanan,¹³ B. L. Hartfiel,¹³ J. W. Gary,¹⁴
J. Layter,¹⁴ B. C. Shen,¹⁴ K. Wang,¹⁴ D. del Re,¹⁵ H. K. Hadavand,¹⁵ E. J. Hill,¹⁵ D. B. MacFarlane,¹⁵
H. P. Paar,¹⁵ Sh. Rahatlou,¹⁵ V. Sharma,¹⁵ J. W. Berryhill,¹⁶ C. Campagnari,¹⁶ B. Dahmes,¹⁶ S. L. Levy,¹⁶
O. Long,¹⁶ A. Lu,¹⁶ M. A. Mazur,¹⁶ J. D. Richman,¹⁶ W. Verkerke,¹⁶ T. W. Beck,¹⁷ J. Beringer,¹⁷ A. M. Eisner,¹⁷
C. A. Heusch,¹⁷ W. S. Lockman,¹⁷ T. Schalk,¹⁷ R. E. Schmitz,¹⁷ B. A. Schumm,¹⁷ A. Seiden,¹⁷ P. Spradlin,¹⁷
W. Walkowiak,¹⁷ D. C. Williams,¹⁷ M. G. Wilson,¹⁷ J. Albert,¹⁸ E. Chen,¹⁸ G. P. Dubois-Felsmann,¹⁸
A. Dvoretzkii,¹⁸ R. J. Erwin,¹⁸ D. G. Hitlin,¹⁸ I. Narsky,¹⁸ T. Piatenko,¹⁸ F. C. Porter,¹⁸ A. Ryd,¹⁸ A. Samuel,¹⁸
S. Yang,¹⁸ S. Jayatilleke,¹⁹ G. Mancinelli,¹⁹ B. T. Meadows,¹⁹ M. D. Sokoloff,¹⁹ T. Abe,²⁰ F. Blanc,²⁰ P. Bloom,²⁰
S. Chen,²⁰ P. J. Clark,²⁰ W. T. Ford,²⁰ U. Nauenberg,²⁰ A. Olivas,²⁰ P. Rankin,²⁰ J. Roy,²⁰ J. G. Smith,²⁰
W. C. van Hoek,²⁰ L. Zhang,²⁰ J. L. Harton,²¹ T. Hu,²¹ A. Soffer,²¹ W. H. Toki,²¹ R. J. Wilson,²¹ J. Zhang,²¹
D. Altenburg,²² T. Brandt,²² J. Brose,²² T. Colberg,²² M. Dickopp,²² E. Feltresi,²² A. Hauke,²² H. M. Lacker,²²
E. Maly,²² R. Müller-Pfefferkorn,²² R. Nogowski,²² S. Otto,²² J. Schubert,²² K. R. Schubert,²² R. Schwierz,²²
B. Spaan,²² D. Bernard,²³ G. R. Bonneaud,²³ F. Brochard,²³ P. Grenier,²³ Ch. Thiebaux,²³ G. Vasileiadis,²³
M. Verderi,²³ D. J. Bard,²⁴ A. Khan,²⁴ D. Lavin,²⁴ F. Muheim,²⁴ S. Playfer,²⁴ M. Andreotti,²⁵ V. Azzolini,²⁵
D. Bettoni,²⁵ C. Bozzi,²⁵ R. Calabrese,²⁵ G. Cibinetto,²⁵ E. Luppi,²⁵ M. Negrini,²⁵ L. Piemontese,²⁵ A. Sarti,²⁵
E. Treadwell,²⁶ R. Baldini-Ferroli,²⁷ A. Calcaterra,²⁷ R. de Sangro,²⁷ G. Finocchiaro,²⁷ P. Patteri,²⁷ M. Piccolo,²⁷
A. Zallo,²⁷ A. Buzzo,²⁸ R. Capra,²⁸ R. Contri,²⁸ G. Crosetti,²⁸ M. Lo Vetere,²⁸ M. Macri,²⁸ M. R. Monge,²⁸
S. Passaggio,²⁸ C. Patrignani,²⁸ E. Robutti,²⁸ A. Santroni,²⁸ S. Tosi,²⁸ S. Bailey,²⁹ M. Morii,²⁹ E. Won,²⁹
R. S. Dubitzky,³⁰ U. Langenegger,³⁰ W. Bhimji,³¹ D. A. Bowerman,³¹ P. D. Dauncey,³¹ U. Egede,³¹
J. R. Gaillard,³¹ G. W. Morton,³¹ J. A. Nash,³¹ G. P. Taylor,³¹ G. J. Grenier,³² S.-J. Lee,³² U. Mallik,³²
J. Cochran,³³ H. B. Crawley,³³ J. Lamsa,³³ W. T. Meyer,³³ S. Prell,³³ E. I. Rosenberg,³³ J. Yi,³³ M. Davier,³⁴
G. Grosdidier,³⁴ A. Höcker,³⁴ S. Laplace,³⁴ F. Le Diberder,³⁴ V. Lepeltier,³⁴ A. M. Lutz,³⁴ T. C. Petersen,³⁴
S. Plaszczynski,³⁴ M. H. Schune,³⁴ L. Tantot,³⁴ G. Wormser,³⁴ V. Brigljević,³⁵ C. H. Cheng,³⁵ D. J. Lange,³⁵
M. C. Simani,³⁵ D. M. Wright,³⁵ A. J. Bevan,³⁶ J. P. Coleman,³⁶ J. R. Fry,³⁶ E. Gabathuler,³⁶ R. Gamet,³⁶
M. Kay,³⁶ R. J. Parry,³⁶ D. J. Payne,³⁶ R. J. Sloane,³⁶ C. Touramanis,³⁶ J. J. Back,³⁷ P. F. Harrison,³⁷
G. B. Mohanty,³⁷ C. L. Brown,³⁸ G. Cowan,³⁸ R. L. Flack,³⁸ H. U. Flaecher,³⁸ S. George,³⁸ M. G. Green,³⁸
A. Kurup,³⁸ C. E. Marker,³⁸ T. R. McMahon,³⁸ S. Ricciardi,³⁸ F. Salvatore,³⁸ G. Vaitsas,³⁸ M. A. Winter,³⁸
D. Brown,³⁹ C. L. Davis,³⁹ J. Allison,⁴⁰ N. R. Barlow,⁴⁰ R. J. Barlow,⁴⁰ P. A. Hart,⁴⁰ M. C. Hodgkinson,⁴⁰
G. D. Lafferty,⁴⁰ A. J. Lyon,⁴⁰ J. C. Williams,⁴⁰ A. Farbin,⁴¹ W. D. Hulsbergen,⁴¹ A. Jawahery,⁴¹ D. Kovalskyi,⁴¹
C. K. Lae,⁴¹ V. Lillard,⁴¹ D. A. Roberts,⁴¹ G. Blaylock,⁴² C. Dallapiccola,⁴² K. T. Flood,⁴² S. S. Hertzbach,⁴²
R. Kofler,⁴² V. B. Koptchev,⁴² T. B. Moore,⁴² S. Saremi,⁴² H. Staengle,⁴² S. Willocq,⁴² R. Cowan,⁴³ G. Sciolla,⁴³
F. Taylor,⁴³ R. K. Yamamoto,⁴³ D. J. J. Mangeol,⁴⁴ P. M. Patel,⁴⁴ S. H. Robertson,⁴⁴ A. Lazzaro,⁴⁵ F. Palombo,⁴⁵

J. M. Bauer,⁴⁶ L. Cremaldi,⁴⁶ V. Eschenburg,⁴⁶ R. Godang,⁴⁶ R. Kroeger,⁴⁶ J. Reidy,⁴⁶ D. A. Sanders,⁴⁶ D. J. Summers,⁴⁶ H. W. Zhao,⁴⁶ S. Brunet,⁴⁷ D. Cote-Ahern,⁴⁷ P. Taras,⁴⁷ H. Nicholson,⁴⁸ C. Cartaro,⁴⁹ N. Cavallo,⁴⁹ G. De Nardo,⁴⁹ F. Fabozzi,^{49,*} C. Gatto,⁴⁹ L. Lista,⁴⁹ P. Paolucci,⁴⁹ D. Piccolo,⁴⁹ C. Sciacca,⁴⁹ M. A. Baak,⁵⁰ G. Raven,⁵⁰ L. Wilden,⁵⁰ C. P. Jessop,⁵¹ J. M. LoSecco,⁵¹ T. A. Gabriel,⁵² T. Allmendinger,⁵³ B. Brau,⁵³ K. K. Gan,⁵³ K. Honscheid,⁵³ D. Hufnagel,⁵³ H. Kagan,⁵³ R. Kass,⁵³ T. Pulliam,⁵³ R. Ter-Antonyan,⁵³ Q. K. Wong,⁵³ J. Brau,⁵⁴ R. Frey,⁵⁴ O. Igonkina,⁵⁴ C. T. Potter,⁵⁴ N. B. Sinev,⁵⁴ D. Strom,⁵⁴ E. Torrence,⁵⁴ F. Colecchia,⁵⁵ A. Dorigo,⁵⁵ F. Galeazzi,⁵⁵ M. Margoni,⁵⁵ M. Morandin,⁵⁵ M. Posocco,⁵⁵ M. Rotondo,⁵⁵ F. Simonetto,⁵⁵ R. Stroili,⁵⁵ G. Tiozzo,⁵⁵ C. Voci,⁵⁵ M. Benayoun,⁵⁶ H. Briand,⁵⁶ J. Chauveau,⁵⁶ P. David,⁵⁶ Ch. de la Vaissière,⁵⁶ L. Del Buono,⁵⁶ O. Hamon,⁵⁶ M. J. J. John,⁵⁶ Ph. Leruste,⁵⁶ J. Ocariz,⁵⁶ M. Pivk,⁵⁶ L. Roos,⁵⁶ S. T'Jampens,⁵⁶ G. Therin,⁵⁶ P. F. Manfredi,⁵⁷ V. Re,⁵⁷ P. K. Behera,⁵⁸ L. Gladney,⁵⁸ Q. H. Guo,⁵⁸ J. Panetta,⁵⁸ F. Anulli,^{27,59} M. Biasini,⁵⁹ I. M. Peruzzi,^{27,59} M. Pioppi,⁵⁹ C. Angelini,⁶⁰ G. Batignani,⁶⁰ S. Bettarini,⁶⁰ M. Bondioli,⁶⁰ F. Bucci,⁶⁰ G. Calderini,⁶⁰ M. Carpinelli,⁶⁰ V. Del Gamba,⁶⁰ F. Forti,⁶⁰ M. A. Giorgi,⁶⁰ A. Lusiani,⁶⁰ G. Marchiori,⁶⁰ F. Martinez-Vidal,^{60,†} M. Morganti,⁶⁰ N. Neri,⁶⁰ E. Paoloni,⁶⁰ M. Rama,⁶⁰ G. Rizzo,⁶⁰ F. Sandrelli,⁶⁰ J. Walsh,⁶⁰ M. Haire,⁶¹ D. Judd,⁶¹ K. Paick,⁶¹ D. E. Wagoner,⁶¹ N. Danielson,⁶² P. Elmer,⁶² C. Lu,⁶² V. Miftakov,⁶² J. Olsen,⁶² A. J. S. Smith,⁶² E. W. Varnes,⁶² F. Bellini,⁶³ G. Cavoto,^{62,63} R. Faccini,⁶³ F. Ferrarotto,⁶³ F. Ferroni,⁶³ M. Gaspero,⁶³ M. A. Mazzoni,⁶³ S. Morganti,⁶³ M. Pierini,⁶³ G. Piredda,⁶³ F. Safai Tehrani,⁶³ C. Voena,⁶³ S. Christ,⁶⁴ G. Wagner,⁶⁴ R. Waldi,⁶⁴ T. Adye,⁶⁵ N. De Groot,⁶⁵ B. Franek,⁶⁵ N. I. Geddes,⁶⁵ G. P. Gopal,⁶⁵ E. O. Olaiya,⁶⁵ S. M. Xella,⁶⁵ R. Aleksan,⁶⁶ S. Emery,⁶⁶ A. Gaidot,⁶⁶ S. F. Ganzhur,⁶⁶ P.-F. Giraud,⁶⁶ G. Hamel de Monchenault,⁶⁶ W. Kozanecki,⁶⁶ M. Langer,⁶⁶ M. Legendre,⁶⁶ G. W. London,⁶⁶ B. Mayer,⁶⁶ G. Schott,⁶⁶ G. Vasseur,⁶⁶ Ch. Yeche,⁶⁶ M. Zito,⁶⁶ M. V. Purohit,⁶⁷ A. W. Weidemann,⁶⁷ F. X. Yumiceva,⁶⁷ D. Aston,⁶⁸ R. Bartoldus,⁶⁸ N. Berger,⁶⁸ A. M. Boyarski,⁶⁸ O. L. Buchmueller,⁶⁸ M. R. Convery,⁶⁸ M. Cristinziani,⁶⁸ D. Dong,⁶⁸ J. Dorfan,⁶⁸ D. Dujmic,⁶⁸ W. Dunwoodie,⁶⁸ E. E. Elsen,⁶⁸ R. C. Field,⁶⁸ T. Glanzman,⁶⁸ S. J. Gowdy,⁶⁸ T. Hadig,⁶⁸ V. Halyo,⁶⁸ T. Hryn'ova,⁶⁸ W. R. Innes,⁶⁸ M. H. Kelsey,⁶⁸ P. Kim,⁶⁸ M. L. Kocian,⁶⁸ D. W. G. S. Leith,⁶⁸ J. Libby,⁶⁸ S. Luitz,⁶⁸ V. Luth,⁶⁸ H. L. Lynch,⁶⁸ H. Marsiske,⁶⁸ R. Messner,⁶⁸ D. R. Muller,⁶⁸ C. P. O'Grady,⁶⁸ V. E. Ozcan,⁶⁸ A. Perazzo,⁶⁸ M. Perl,⁶⁸ S. Petrak,⁶⁸ B. N. Ratcliff,⁶⁸ A. Roodman,⁶⁸ A. A. Salnikov,⁶⁸ R. H. Schindler,⁶⁸ J. Schwiening,⁶⁸ G. Simi,⁶⁸ A. Snyder,⁶⁸ A. Soha,⁶⁸ J. Stelzer,⁶⁸ D. Su,⁶⁸ M. K. Sullivan,⁶⁸ J. Va'vra,⁶⁸ S. R. Wagner,⁶⁸ M. Weaver,⁶⁸ A. J. R. Weinstein,⁶⁸ W. J. Wisniewski,⁶⁸ D. H. Wright,⁶⁸ C. C. Young,⁶⁸ P. R. Burchat,⁶⁹ A. J. Edwards,⁶⁹ T. I. Meyer,⁶⁹ B. A. Petersen,⁶⁹ C. Roat,⁶⁹ M. Ahmed,⁷⁰ S. Ahmed,⁷⁰ M. S. Alam,⁷⁰ J. A. Ernst,⁷⁰ M. A. Saeed,⁷⁰ M. Saleem,⁷⁰ F. R. Wappler,⁷⁰ W. Bugg,⁷¹ M. Krishnamurthy,⁷¹ S. M. Spanier,⁷¹ R. Eckmann,⁷² H. Kim,⁷² J. L. Ritchie,⁷² A. Satpathy,⁷² R. F. Schwitters,⁷² J. M. Izen,⁷³ I. Kitayama,⁷³ X. C. Lou,⁷³ S. Ye,⁷³ F. Bianchi,⁷⁴ M. Bona,⁷⁴ F. Gallo,⁷⁴ D. Gamba,⁷⁴ C. Borean,⁷⁵ L. Bosisio,⁷⁵ F. Cossutti,⁷⁵ G. Della Ricca,⁷⁵ S. Dittongo,⁷⁵ S. Grancagnolo,⁷⁵ L. Lancieri,⁷⁵ P. Poropat,^{75,‡} L. Vitale,⁷⁵ G. Vuagnin,⁷⁵ R. S. Panvini,⁷⁶ Sw. Banerjee,⁷⁷ C. M. Brown,⁷⁷ D. Fortin,⁷⁷ P. D. Jackson,⁷⁷ R. Kowalewski,⁷⁷ J. M. Roney,⁷⁷ H. R. Band,⁷⁸ S. Dasu,⁷⁸ M. Datta,⁷⁸ A. M. Eichenbaum,⁷⁸ J. R. Johnson,⁷⁸ P. E. Kutter,⁷⁸ H. Li,⁷⁸ R. Liu,⁷⁸ F. Di Lodovico,⁷⁸ A. Mihalyi,⁷⁸ A. K. Mohapatra,⁷⁸ Y. Pan,⁷⁸ R. Prepost,⁷⁸ S. J. Sekula,⁷⁸ J. H. von Wimmersperg-Toeller,⁷⁸ J. Wu,⁷⁸ S. L. Wu,⁷⁸ Z. Yu,⁷⁸ and H. Neal⁷⁹

(The BABAR Collaboration)

¹Laboratoire de Physique des Particules, F-74941 Annecy-le-Vieux, France

²Università di Bari, Dipartimento di Fisica and INFN, I-70126 Bari, Italy

³Institute of High Energy Physics, Beijing 100039, China

⁴University of Bergen, Inst. of Physics, N-5007 Bergen, Norway

⁵Lawrence Berkeley National Laboratory and University of California, Berkeley, CA 94720, USA

⁶University of Birmingham, Birmingham, B15 2TT, United Kingdom

⁷Ruhr Universität Bochum, Institut für Experimentalphysik 1, D-44780 Bochum, Germany

⁸University of Bristol, Bristol BS8 1TL, United Kingdom

⁹University of British Columbia, Vancouver, BC, Canada V6T 1Z1

¹⁰Brunel University, Uxbridge, Middlesex UB8 3PH, United Kingdom

¹¹Budker Institute of Nuclear Physics, Novosibirsk 630090, Russia

¹²University of California at Irvine, Irvine, CA 92697, USA

¹³University of California at Los Angeles, Los Angeles, CA 90024, USA

¹⁴University of California at Riverside, Riverside, CA 92521, USA

¹⁵University of California at San Diego, La Jolla, CA 92093, USA

¹⁶University of California at Santa Barbara, Santa Barbara, CA 93106, USA

¹⁷University of California at Santa Cruz, Institute for Particle Physics, Santa Cruz, CA 95064, USA

¹⁸California Institute of Technology, Pasadena, CA 91125, USA

- ¹⁹University of Cincinnati, Cincinnati, OH 45221, USA
²⁰University of Colorado, Boulder, CO 80309, USA
²¹Colorado State University, Fort Collins, CO 80523, USA
²²Technische Universität Dresden, Institut für Kern- und Teilchenphysik, D-01062 Dresden, Germany
²³Ecole Polytechnique, LLR, F-91128 Palaiseau, France
²⁴University of Edinburgh, Edinburgh EH9 3JZ, United Kingdom
²⁵Università di Ferrara, Dipartimento di Fisica and INFN, I-44100 Ferrara, Italy
²⁶Florida A&M University, Tallahassee, FL 32307, USA
²⁷Laboratori Nazionali di Frascati dell'INFN, I-00044 Frascati, Italy
²⁸Università di Genova, Dipartimento di Fisica and INFN, I-16146 Genova, Italy
²⁹Harvard University, Cambridge, MA 02138, USA
³⁰Universität Heidelberg, Physikalisches Institut, Philosophenweg 12, D-69120 Heidelberg, Germany
³¹Imperial College London, London, SW7 2AZ, United Kingdom
³²University of Iowa, Iowa City, IA 52242, USA
³³Iowa State University, Ames, IA 50011-3160, USA
³⁴Laboratoire de l'Accélérateur Linéaire, F-91898 Orsay, France
³⁵Lawrence Livermore National Laboratory, Livermore, CA 94550, USA
³⁶University of Liverpool, Liverpool L69 3BX, United Kingdom
³⁷Queen Mary, University of London, E1 4NS, United Kingdom
³⁸University of London, Royal Holloway and Bedford New College, Egham, Surrey TW20 0EX, United Kingdom
³⁹University of Louisville, Louisville, KY 40292, USA
⁴⁰University of Manchester, Manchester M13 9PL, United Kingdom
⁴¹University of Maryland, College Park, MD 20742, USA
⁴²University of Massachusetts, Amherst, MA 01003, USA
⁴³Massachusetts Institute of Technology, Laboratory for Nuclear Science, Cambridge, MA 02139, USA
⁴⁴McGill University, Montréal, QC, Canada H3A 2T8
⁴⁵Università di Milano, Dipartimento di Fisica and INFN, I-20133 Milano, Italy
⁴⁶University of Mississippi, University, MS 38677, USA
⁴⁷Université de Montréal, Laboratoire René J. A. Lévesque, Montréal, QC, Canada H3C 3J7
⁴⁸Mount Holyoke College, South Hadley, MA 01075, USA
⁴⁹Università di Napoli Federico II, Dipartimento di Scienze Fisiche and INFN, I-80126, Napoli, Italy
⁵⁰NIKHEF, National Institute for Nuclear Physics and High Energy Physics, NL-1009 DB Amsterdam, The Netherlands
⁵¹University of Notre Dame, Notre Dame, IN 46556, USA
⁵²Oak Ridge National Laboratory, Oak Ridge, TN 37831, USA
⁵³Ohio State University, Columbus, OH 43210, USA
⁵⁴University of Oregon, Eugene, OR 97403, USA
⁵⁵Università di Padova, Dipartimento di Fisica and INFN, I-35131 Padova, Italy
⁵⁶Universités Paris VI et VII, Lab de Physique Nucléaire H. E., F-75252 Paris, France
⁵⁷Università di Pavia, Dipartimento di Elettronica and INFN, I-27100 Pavia, Italy
⁵⁸University of Pennsylvania, Philadelphia, PA 19104, USA
⁵⁹Università di Perugia, Dipartimento di Fisica and INFN, I-06100 Perugia, Italy
⁶⁰Università di Pisa, Dipartimento di Fisica, Scuola Normale Superiore and INFN, I-56127 Pisa, Italy
⁶¹Prairie View A&M University, Prairie View, TX 77446, USA
⁶²Princeton University, Princeton, NJ 08544, USA
⁶³Università di Roma La Sapienza, Dipartimento di Fisica and INFN, I-00185 Roma, Italy
⁶⁴Universität Rostock, D-18051 Rostock, Germany
⁶⁵Rutherford Appleton Laboratory, Chilton, Didcot, Oxon, OX11 0QX, United Kingdom
⁶⁶DSM/Dapnia, CEA/Saclay, F-91191 Gif-sur-Yvette, France
⁶⁷University of South Carolina, Columbia, SC 29208, USA
⁶⁸Stanford Linear Accelerator Center, Stanford, CA 94309, USA
⁶⁹Stanford University, Stanford, CA 94305-4060, USA
⁷⁰State Univ. of New York, Albany, NY 12222, USA
⁷¹University of Tennessee, Knoxville, TN 37996, USA
⁷²University of Texas at Austin, Austin, TX 78712, USA
⁷³University of Texas at Dallas, Richardson, TX 75083, USA
⁷⁴Università di Torino, Dipartimento di Fisica Sperimentale and INFN, I-10125 Torino, Italy
⁷⁵Università di Trieste, Dipartimento di Fisica and INFN, I-34127 Trieste, Italy
⁷⁶Vanderbilt University, Nashville, TN 37235, USA
⁷⁷University of Victoria, Victoria, BC, Canada V8W 3P6
⁷⁸University of Wisconsin, Madison, WI 53706, USA
⁷⁹Yale University, New Haven, CT 06511, USA

(Dated: November 6, 2003)

We have observed the rare decay $B^0 \rightarrow \rho^+ \rho^-$ in a sample of 89 million $B\bar{B}$ pairs recorded with the *BABAR* detector. The number of observed events is $88_{-21}^{+23} \pm 9$, with a significance of 5.1 standard deviations with systematic uncertainties included. The branching fraction and the longitudinal polarization are measured to be $\mathcal{B}(B^0 \rightarrow \rho^+ \rho^-) = (25_{-6}^{+7+5}) \times 10^{-6}$ and $\Gamma_L/\Gamma = 0.98_{-0.08}^{+0.02} \pm 0.03$, respectively.

PACS numbers: 13.25.Hw, 11.30.Er, 12.15.Hh

Charmless B -meson decays provide an opportunity to measure the angles of the unitary triangles constructed from the elements of the Cabibbo-Kobayashi-Maskawa (CKM) quark-mixing matrix [1]. There has been interest in the study of $B \rightarrow \pi\pi$ and $\rho\pi$ decays, where the time-dependent CP -violating asymmetries are related to the CKM angle $\alpha \equiv \arg[-V_{td}V_{tb}^*/V_{ud}V_{ub}^*]$, and interference between tree and loop (penguin) amplitudes could give rise to direct CP violation. The decay $B^0 \rightarrow \rho^+ \rho^-$ is another promising mode for CP -violation studies and has the advantage of a larger expected decay rate and smaller uncertainty in penguin contributions. The measurements of the amplitudes in B decays to two vector particles provide additional tests of theoretical calculations [2, 3, 4].

The decay $B^0 \rightarrow \rho^+ \rho^-$ is expected to proceed through the tree-level $b \rightarrow u$ transition and through CKM-suppressed $b \rightarrow d$ penguin transitions, as illustrated in Fig. 1 [4, 5]. The extraction of α from measurements made with this decay requires an understanding of the contributing amplitudes. It also requires proper accounting for CP -even (S- and D-wave) and CP -odd (P-wave) components in the decay amplitude. The recent limit on the $B^0 \rightarrow \rho^0 \rho^0$ decay rate [6] and the measurements of the $B^+ \rightarrow \rho^+ \rho^0$ branching fraction [6, 7] place experimental limits on the contribution of penguin amplitudes. Measurements of the longitudinal polarization, defined as the ratio between the longitudinal and total decay rates $f_L \equiv \Gamma_L/\Gamma$ [2], in the $B^+ \rightarrow \rho^+ \rho^0$ decay provide evidence that the CP -even component dominates in $B \rightarrow \rho\rho$ decays [6, 7].

In this paper we report the observation of the $B^0 \rightarrow \rho^+ \rho^-$ decay mode and measurements of its branching fraction and the amount of longitudinal polarization in the decay. We also make a quantitative estimate of penguin contributions in this decay using our earlier measurements in isospin-related $B \rightarrow \rho\rho$ modes.

We use data collected with the *BABAR* detector [8] at the PEP-II asymmetric-energy e^+e^- storage ring. These data represent an integrated luminosity of 81.9 fb^{-1} at the e^+e^- center-of-mass (CM) energy of the $\Upsilon(4S)$ resonance ($\sqrt{s} = 10.58 \text{ GeV}$, on-resonance), corresponding to 88.9 million $B\bar{B}$ pairs, and 9.6 fb^{-1} approximately 40 MeV below this energy (off-resonance).

Charged-particle momenta are measured in a tracking system consisting of a five-layer double-sided silicon vertex tracker (SVT) and a 40-layer central drift chamber (DCH), both situated in a 1.5-T axial magnetic field.

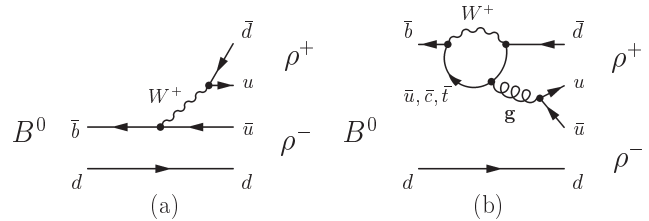


FIG. 1: Diagrams describing the decay $B^0 \rightarrow \rho^+ \rho^-$: (a) dominant tree diagram, (b) gluonic penguin diagram.

BABAR achieves an impact parameter resolution of about $40 \mu\text{m}$ for the high-momentum charged particles from the B decay, allowing the precise determination of decay vertices. The tracking system covers 92% of the solid angle in the CM frame.

Charged-particle identification is provided by measurements of energy loss (dE/dx) in the tracking devices (SVT and DCH) and by an internally reflecting ring-imaging Cherenkov detector (DIRC). A K - π separation of better than four standard deviations (σ) is achieved for momenta below 3 GeV, decreasing to 2.5σ at the highest momenta in the B decay final states. Photons are detected by a CsI(Tl) electromagnetic calorimeter (EMC). The EMC provides good energy and angular resolution for detection of photons with energy in the range 20 MeV to 4 GeV. The energy and angular resolutions are 3% and 4 mrad, respectively, for a 1 GeV photon.

Hadronic events are selected based on track multiplicity and event topology. We fully reconstruct $B^0 \rightarrow \rho^+ \rho^-$ candidates from the decay products of the $\rho^\pm \rightarrow \pi^\pm \pi^0$ and $\pi^0 \rightarrow \gamma\gamma$ decays. Charged-track candidates are required to originate from the interaction point, have at least 12 DCH hits and have a minimum transverse momentum of 0.1 GeV. Charged-pion tracks are distinguished from kaon and proton tracks with a likelihood ratio that includes dE/dx information from the SVT and DCH, and, for momenta above 0.7 GeV, the Cherenkov angle and number of photons measured by the DIRC. Charged pions are distinguished from electrons primarily on the basis of their EMC shower energy and spatial profile.

We reconstruct π^0 mesons from pairs of photons. Photon candidates are required to have a minimum energy of 30 MeV, have a shower shape consistent with the photon hypothesis, and not be matched to a track. The typi-

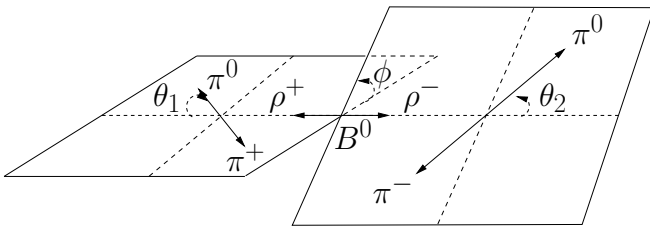


FIG. 2: Definition of helicity angles θ_1 , θ_2 , and ϕ , for the decay $B^0 \rightarrow \rho^+ \rho^-$. The $\pi^\pm \pi^0$ final states are shown in the ρ^\pm rest frames.

cal experimental resolution for the measured π^0 mass is 7 MeV. We require π^0 candidates to have an invariant mass within 15 MeV of the true π^0 mass. The invariant mass of the ρ^\pm candidate ($m_{\pi^\pm \pi^0}$) is required to be in the range 0.52 to 1.02 GeV. The helicity angles θ_1 and θ_2 of ρ^+ and ρ^- are defined as the angles between the π^0 direction and the direction opposite the B in each ρ rest frame as shown in Fig. 2. The helicity angles are restricted to the region $-0.75 \leq \cos \theta_{1,2} \leq 0.95$ to suppress combinatorial background and reduce acceptance uncertainties due to low-momentum pion reconstruction.

The B meson candidates are identified from two nearly independent kinematic observables [8], the beam energy-substituted mass $m_{\text{ES}} = [(s/2 + \mathbf{p}_i \cdot \mathbf{p}_B)^2 / E_i^2 - \mathbf{p}_B^2]^{1/2}$ and the energy difference $\Delta E = (E_i E_B - \mathbf{p}_i \cdot \mathbf{p}_B - s/2) / \sqrt{s}$, where (E_i, \mathbf{p}_i) is the e^+e^- initial state four-momentum, and (E_B, \mathbf{p}_B) is the four-momentum of the reconstructed B candidate, all defined in the laboratory frame. For signal events, the m_{ES} distribution peaks at the B mass and the ΔE distribution peaks near zero. Our selection requires $m_{\text{ES}} > 5.2$ GeV and $|\Delta E| < 0.2$ GeV, while the signal resolution is roughly 3 MeV and 50 MeV, respectively. The sideband regions are defined as $5.2 \text{ GeV} < m_{\text{ES}} < 5.27 \text{ GeV}$ or $0.1 \text{ GeV} < |\Delta E| < 0.2 \text{ GeV}$.

To reject the dominant continuum background (from $e^+e^- \rightarrow q\bar{q}$ events, $q = u, d, s, c$), we require $|\cos \theta_T| < 0.8$, where θ_T is the angle between the thrust axis of the B candidate and the thrust axis of the rest of the tracks and photon candidates in the event, calculated in the CM frame. The distribution of $|\cos \theta_T|$ is sharply peaked near 1.0 for jet-like events originating from $q\bar{q}$ pairs and nearly uniform for the isotropic decays of the B meson. A Fisher discriminant (\mathcal{F}) combines 11 observables: the polar angle of the B momentum vector and the polar angle of the B -candidate thrust axis, both calculated with respect to the beam axis in the CM frame, and the scalar sum of the CM momenta of charged particles and photons (excluding particles from the B candidate) entering nine coaxial angular intervals of 10° around the B -candidate thrust axis [9].

The selected sample contains 54,042 events most of

which populate sidebands of the observables. Background from other B decays is estimated with Monte Carlo (MC) simulation [10]; it contributes 5% of the events in the selected sample. This background component, arising mainly from $b \rightarrow c$ transitions, is explicitly included in the fit described below.

We use an unbinned, extended maximum-likelihood fit to extract simultaneously the signal yield and polarization. There are three event categories j : signal, continuum $q\bar{q}$, and $B\bar{B}$ combinatorial background. The likelihood for each $B^0 \rightarrow \rho^+ \rho^-$ candidate i is defined as

$$\mathcal{L}_i = \sum_{j=1}^3 n_j \mathcal{P}_j(\vec{x}_i; \vec{\beta}), \quad (1)$$

where each of the $\mathcal{P}_j(\vec{x}_i; \vec{\beta})$ is the probability density function (PDF) for seven observables \vec{x}_i (m_{ES} , ΔE , \mathcal{F} , $m_{\pi^+ \pi^0}$, $m_{\pi^- \pi^0}$, θ_1 , θ_2) and is described by the PDF parameters $\vec{\beta}$. The event yields n_j for each category j are free parameters in the fit. We allow for multiple candidates in a given event by assigning to each selected candidate a weight of $1/N_i$, where N_i is the number of candidates in that event. The average number of candidates per event is 1.27. MC simulation shows that this procedure does not introduce bias while providing a small statistical improvement over the random choice of a candidate in a given event. The extended likelihood for a sample of N_{cand} candidates is

$$\mathcal{L} = \exp \left(- \sum_{j=1}^3 n_j \right) \prod_{i=1}^{N_{\text{cand}}} \exp \left(\frac{\ln \mathcal{L}_i}{N_i} \right). \quad (2)$$

The correlations among the input observables \vec{x}_i are found to be small for both the background ($< 5\%$) and signal ($< 10\%$), except for angular correlations in the signal. The $\mathcal{P}_j(\vec{x}_i; \vec{\beta})$, for a given candidate i , is the product of PDFs for each of the observables and a joint PDF for the helicity angles, which accounts for the angular correlations in the signal and for detector acceptance effects. We integrate over the angle ϕ between the two decay planes shown in Fig. 2, leaving a PDF that depends only on θ_1 , θ_2 , and the unknown longitudinal polarization f_L . The differential decay rate [2] is

$$\frac{1}{\Gamma} \frac{d^2 \Gamma}{d \cos \theta_1 d \cos \theta_2} = \frac{9}{4} \left\{ \frac{1}{4} (1 - f_L) \sin^2 \theta_1 \sin^2 \theta_2 + f_L \cos^2 \theta_1 \cos^2 \theta_2 \right\}. \quad (3)$$

The PDF parameters $\vec{\beta}$, except for f_L , are extracted from MC simulation and on-resonance m_{ES} and ΔE sidebands, and are fixed in the fit. The resolutions are adjusted by comparing data and simulation in calibration channels with similar kinematics and topology, such as $B \rightarrow \bar{D} \rho^+, \bar{D} \pi^+$ with $\bar{D} \rightarrow$

$K^+\pi^-(\pi^0), K^0\pi^-(\pi^0), K^+\pi^-\pi^-, K^0\pi^-\pi^+$. To describe the signal distributions, we use Gaussian functions for the parameterization of the PDFs for m_{ES} and ΔE , and a relativistic P-wave Breit-Wigner distribution for the ρ^\pm resonance masses. The angular acceptance effects are parameterized with empirical polynomial functions for each helicity angle and are included in the joint helicity-angle PDF as a factor multiplying the ideal distribution in Eq. (3).

For the background PDFs, we use polynomials or, in the case of m_{ES} , an empirical phase-space function [11]. In the background PDF we incorporate a small linear correlation between the curvature ξ of the phase-space function and the value of \mathcal{F} . The background parameterizations for the ρ^\pm candidate masses also include a resonant component to account for ρ^\pm production. The background helicity-angle distribution is also separated into contributions from combinatorial background and from real ρ^\pm mesons, both described by polynomials. For both signal and background, the PDF for \mathcal{F} is represented by a Gaussian distribution with different widths above and below the peak.

PDF parameters for the background from other B decays are determined from MC simulation. The contribution from charmless B decays with similar topology (cross-feed modes) such as $B \rightarrow \rho\pi, \rho^0\rho^+, \rho K^*, a_1\pi$, and $a_1\rho$ is estimated with MC modeling and is fixed in the fit. Each branching fraction for the cross-feed modes is estimated to be in the range $(1-3) \times 10^{-5}$. The branching fractions for these and many other modes are taken from the most recent measurements [6, 7, 12] or extrapolated from other results with a flavor-SU(3)-symmetry approximation.

The selected $B^0 \rightarrow \rho^+\rho^-$ events fall into three categories. MC simulation of events with longitudinal polarization shows that roughly 30% of the events contain only misreconstructed candidates. Approximately 20% of the events contain both correctly and incorrectly reconstructed candidates. The remainder contain only correct candidates. Misreconstruction occurs when at least one candidate photon in a π^0 candidate or one charged track in a ρ candidate belongs to the decay products of the other B . The distributions that show peaks for correctly reconstructed events have substantial tails, with large uncertainties in MC simulation, when misreconstructed events are included. These tails would reduce the power of the distributions to discriminate between the background and the collection of correctly and incorrectly reconstructed events. We choose, therefore, to represent only the correctly reconstructed candidates in the signal PDF. Misreconstructed candidates are predominantly accommodated by the combinatorial background PDF. Fitting to determine the number of correctly reconstructed candidates has an efficiency less than 100% since some fraction of the events have both correctly and incorrectly reconstructed candidates. Monte Carlo simu-

TABLE I: Summary of the fit results; n_{sig} is the fitted number of signal events, \mathcal{S} is the significance, f_L is the longitudinal polarization, ε denotes the reconstruction efficiency, and \mathcal{B} is the branching fraction of the $B^0 \rightarrow \rho^+\rho^-$ decays. The first uncertainty is statistical and the second systematic. The efficiency (ε) and significance (\mathcal{S}) include systematic uncertainties, and the significance without systematics is given in parentheses.

Quantity	Measured Value
n_{sig}	$88_{-21}^{+23} \pm 9$
\mathcal{S}	$5.1 \sigma (5.5 \sigma)$
f_L	$0.98_{-0.08}^{+0.02} \pm 0.03$
ε	$3.9_{-0.6}^{+0.9} \%$
\mathcal{B}	$(25_{-6}^{+7} {}_{-6}^{+5}) \times 10^{-6}$

lation finds this efficiency to be 87%.

In this analysis, we do not include a fit component for other B decays with the same final-state particles selected within the ρ resonance mass window, such as non-resonant decays $B^0 \rightarrow \pi^+\pi^-\pi^0\pi^0$ and $B^0 \rightarrow \rho^\pm\pi^\mp\pi^0$. The contribution of these decays to the fit results is significantly suppressed by the selection requirements on the masses and by the mass and helicity-angle information in the fit; they are examined in the context of mass and helicity-angle distributions, as discussed below.

The event yields n_j and polarization f_L are obtained by minimizing the quantity $\chi^2 \equiv -2 \ln \mathcal{L}$. The dependence of χ^2 on a fit parameter n_j or f_L is obtained with the other fit parameters floating. Their values are constrained to the physical range $n_j \geq 0$ and $0 \leq f_L \leq 1$. Statistical uncertainties correspond to a unit increase in χ^2 . The statistical significance of the signal is defined as the square root of the change in χ^2 when the number of signal events is constrained to zero in the likelihood fit.

The results of our maximum-likelihood fits are summarized in Table I. The statistical significance of the $B^0 \rightarrow \rho^+\rho^-$ signal is 5.5σ . We find that the ρ^\pm mesons in $B^0 \rightarrow \rho^+\rho^-$ decays are almost fully longitudinally polarized. To compute the branching fraction, equal production rates for $B^0\bar{B}^0$ and B^+B^- are assumed. To check the stability of our results we refit, removing each observable from the fit in turn, and find consistent results. The measured uncertainties in the number of fitted events and the polarization, the statistical significance, and the fit χ^2 value are well reproduced with generated MC samples.

The projections of the fit input observables are shown in Fig. 3. The projections are made after a requirement on the signal-to-background probability ratio $\mathcal{P}_{\text{sig}}(\vec{x}_i; \vec{\beta})/\mathcal{P}_{\text{bkg}}(\vec{x}_i; \vec{\beta})$, where \mathcal{P}_{sig} and \mathcal{P}_{bkg} are the signal and the dominant continuum background PDFs de-

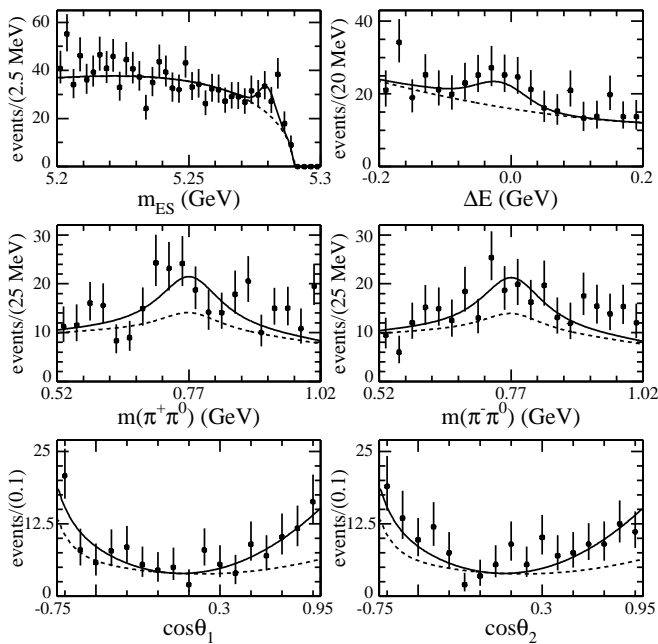


FIG. 3: Projections onto the observables m_{ES} , ΔE , $m_{\pi^+\pi^0}$, $m_{\pi^-\pi^0}$, $\cos\theta_1$, and $\cos\theta_2$ after a requirement on the signal-to-background probability ratio $\mathcal{P}_{\text{sig}}/\mathcal{P}_{\text{bkg}}$ with the PDF for the plotted observable excluded. The points with error bars show the data, the solid (dashed) line shows the signal-plus-background (background only) PDF projection.

defined in Eq. (1), but with the PDF for the plotted observable excluded. The points with error bars show the data with (40–60)% of signal retained, while the lines show the corresponding PDF projections.

To check the sensitivity of our results to the presence of nonresonant $B^0 \rightarrow \pi^+\pi^-\pi^0\pi^0$ and $B^0 \rightarrow \rho^\pm\pi^\mp\pi^0$ decays, we explicitly include a fit component for them, assuming a phase-space decay model. The selection requirements alone suppress the $B \rightarrow 4\pi$ ($B \rightarrow \rho\pi\pi$) efficiency by two (one) orders of magnitude relative to $B^0 \rightarrow \rho^+\rho^-$. The fit results with a nonresonant component indicate a potential $B \rightarrow \rho\pi\pi$ contribution of $(10 \pm 10)\%$ (statistical uncertainty only) of our nominal $B^0 \rightarrow \rho^+\rho^-$ event yield in Table I; interference effects between the resonant and nonresonant components were ignored in this fit. The hypothesis that all the signal is nonresonant $B \rightarrow 4\pi$ ($B \rightarrow \rho\pi\pi$) is excluded with 5.1σ (4.4σ) statistical significance. These results are consistent with our assumption that the nonresonant contribution is negligible.

The systematic uncertainty in the fitted number of signal events (n_{sig}) originates from the uncertainty in the cross-feed B -decay modeling, which was studied with MC generated samples and estimated to be half of the variation with cross-feed set to zero (3% uncertainty in n_{sig}). Systematic uncertainties in the fit originate from assumptions about the PDF parameters. Uncertainties in the

PDF parameters arise from the limited number of events in the background sideband data and signal control samples. We vary them within their respective uncertainties, and derive the associated systematic uncertainty on the event yield (9%). The signal remains statistically significant with these variations (5.1σ including systematics).

The systematic uncertainties in the efficiency (ε) are due to track finding (2% for two tracks), particle identification (2% for two tracks), and π^0 reconstruction (13% for two π^0 s). The fit efficiency is less than 100% because of misreconstructed signal events. This has an additional systematic uncertainty due to uncertainties in the modeling of misreconstructed events. We account for this with a systematic uncertainty on the efficiency of 7%, which is half of the inefficiency; the fit efficiency cannot exceed 100% and the frequency of multiple candidate selection is estimated in the B decay control samples. The reconstruction efficiency depends on the decay polarization. We calculate the efficiencies using the measured polarization and assign a systematic uncertainty ($^{+17}_{-3}\%$) corresponding to the total polarization measurement uncertainty. Smaller systematic uncertainties arise from event-selection criteria, MC statistics, and the number of produced B mesons.

For the polarization measurement (f_L), we include systematic uncertainties from PDF variations that account for uncertainties in the detector acceptance, estimated with MC, and background parameterizations. This results in a total absolute uncertainty of 0.025. The biases from the resolution in helicity-angle measurement and dilution due to the presence of the misreconstructed combinations are studied with MC simulation and give a systematic uncertainty of 0.02.

Observation of the $B^0 \rightarrow \rho^+\rho^-$ decay completes a first set of measurements of the isospin-related $B \rightarrow \rho\rho$ modes [6, 7]. The measured branching fraction is consistent with recent predicted values in the range $(18\text{--}35) \times 10^{-6}$ [4] and the dominant longitudinal polarization implies a suppression of the transverse amplitude, which is expected to be suppressed by a factor of m_ρ/m_B [4]. The rates of the $B^0 \rightarrow \rho^+\rho^-$ and $B^+ \rightarrow \rho^0\rho^+$ decays appear to be larger than the corresponding rates of $B \rightarrow \pi\pi$ decays [12]. At the same time, the recent measurement of the $B^+ \rightarrow \rho^0 K^{*+}$ branching fraction [6] does not show significant enhancement with respect to $B \rightarrow \pi K$ decays [12], both of which are expected to be dominated by $b \rightarrow s$ penguin diagrams. We can use flavor SU(3) to relate $b \rightarrow s$ and $b \rightarrow d$ penguins analogous to Fig. 1(b) [13]; the measured branching fractions indicate that the relative penguin contributions in the $B \rightarrow \rho\rho$ decays are smaller than in the $B \rightarrow \pi\pi$ case.

We make a more quantitative estimate of penguin contributions in $B \rightarrow \rho\rho$ decays using our previous measurements of $B^0 \rightarrow \rho^0\rho^0$ and $B^+ \rightarrow \rho^+\rho^0$ branching fractions and polarization [6]. Since the tree contribution to the $B^0 \rightarrow \rho^0\rho^0$ decay is color-suppressed, the decay rate is

sensitive to the penguin diagram analogous to Fig. 1(b). Using the earlier *BABAR* measurements [6], we obtain a 90% confidence level (C.L.) upper limit on the ratio of the longitudinal amplitudes A_L in the $B \rightarrow \rho\rho$ decays:

$$\frac{|A_L(B^0 \rightarrow \rho^0\rho^0)|^2 + |A_L(\bar{B}^0 \rightarrow \rho^0\rho^0)|^2}{2 \times |A_L(B^+ \rightarrow \rho^0\rho^+)|^2} = \frac{\mathcal{B}(B^0 \rightarrow \rho^0\rho^0) \times f_L(B^0 \rightarrow \rho^0\rho^0)}{\mathcal{B}(B^+ \rightarrow \rho^0\rho^+) \times f_L(B^+ \rightarrow \rho^0\rho^+)} < 0.10. \quad (4)$$

In the above calculation we conservatively assume that the $B^0 \rightarrow \rho^0\rho^0$ decay polarization is fully longitudinal ($f_L = 1$), use the average branching fraction measurements for the B and \bar{B} decays, and assume $|A_L(B^+ \rightarrow \rho^0\rho^+)| = |A_L(B^- \rightarrow \rho^0\rho^-)|$ with only a tree-diagram contribution. The limit in Eq. (4) corresponds to a 19° uncertainty (at 90% C.L.) on α due to penguin contributions in the time-dependent measurements with longitudinally-polarized $B^0 \rightarrow \rho^+\rho^-$ decays, assuming isospin relations analogous to those discussed in the context of $B \rightarrow \pi\pi$ [14] and neglecting the nonresonant and $I = 1$ isospin contributions [15].

In summary, we have observed the decay $B^0 \rightarrow \rho^+\rho^-$, measured its branching fraction $\mathcal{B} = (25_{-6}^{+7+5}) \times 10^{-6}$, and determined the longitudinal polarization fraction $f_L = 0.98_{-0.08}^{+0.02} \pm 0.03$. Our quantitative estimates of penguin contributions in $B^0 \rightarrow \rho^+\rho^-$ decays and the dominance of the CP -even longitudinal polarization make this decay a promising channel for the measurement of the CKM angle α .

We are grateful for the excellent luminosity and machine conditions provided by our PEP-II colleagues, and for the substantial dedicated effort from the computing organizations that support *BABAR*. The collaborating institutions wish to thank SLAC for its support and kind hospitality. This work is supported by DOE and NSF (USA), NSERC (Canada), IHEP (China), CEA and CNRS-IN2P3 (France), BMBF and DFG (Germany), INFN (Italy), FOM (The Netherlands), NFR (Norway), MIST (Russia), and PPARC (United Kingdom). Individuals have received support from the A. P. Sloan Foun-

ation, Research Corporation, and Alexander von Humboldt Foundation.

* Also with Università della Basilicata, Potenza, Italy

† Also with IFIC, Instituto de Física Corpuscular, CSIC-Universidad de Valencia, Valencia, Spain

‡ Deceased

- [1] N. Cabibbo, Phys. Rev. Lett. **10**, 531 (1963); M. Kobayashi and T. Maskawa, Prog. Theor. Phys. **49**, 652 (1973).
- [2] G. Kramer and W.F. Palmer, Phys. Rev. D **45**, 193 (1992).
- [3] R. Aleksan *et al.*, Phys. Lett. B **356**, 95 (1995).
- [4] D. Ebert, R.N. Faustov, and V.O. Galkin, Phys. Rev. D **56**, 312 (1997); A. Ali, G. Kramer, and C.-D. Lu, Phys. Rev. D **58**, 094009 (1998); Y.-H. Chen *et al.*, Phys. Rev. D **60**, 094014 (1999); H.-Y. Cheng and K.-C. Yang, Phys. Lett. B **511**, 40 (2001).
- [5] We use the name of one member of a charge conjugate pair to refer to both unless explicitly stated otherwise.
- [6] *BABAR* Collaboration, B. Aubert *et al.*, Phys. Rev. Lett. **91**, 171802 (2003).
- [7] Belle Collaboration, J. Zhang *et al.*, hep-ex/0306007, submitted to Phys. Rev. Lett. (2003).
- [8] *BABAR* Collaboration, B. Aubert *et al.*, Nucl. Instrum. Methods **A479**, 1 (2002).
- [9] CLEO Collaboration, D.M. Asner *et al.*, Phys. Rev. D **53**, 1039 (1996).
- [10] The *BABAR* detector Monte Carlo simulation is based on GEANT4: S. Agostinelli *et al.*, Nucl. Instrum. Methods **A506**, 250 (2003).
- [11] With $x \equiv 2m_{ES}/\sqrt{s}$ and ξ a parameter to be fit, $f(x) \propto x\sqrt{1-x^2} \exp[-\xi(1-x^2)]$; see ARGUS Collaboration, H. Albrecht *et al.*, Phys. Lett. B **241**, 278 (1990).
- [12] Particle Data Group, K. Hagiwara *et al.*, Phys. Rev. D **66**, 010001 (2002).
- [13] M. Gronau and J.L. Rosner, Phys. Rev. D **65**, 013004 (2002).
- [14] M. Gronau and D. London, Phys. Rev. Lett. **65**, 3381 (1990); Y. Grossman and H. Quinn, Phys. Rev. D **58**, 017504 (1998).
- [15] A.F. Falk *et al.*, hep-ph/0310242, submitted to Phys. Rev. D (2003).